


Original Research

# Sanguinarine Triggers Apoptosis in Cutaneous Squamous Cell Carcinoma Cells through Reactive Oxygen Species-Dependent c-Jun N-Terminal Kinase Signaling Pathway

Kalyani Patil<sup>1</sup>, Abdul Q Khan<sup>1</sup>, Fareed Ahmad<sup>1,2</sup>, Shilpa Kuttikrishnan<sup>1</sup>, Rasheeda Anver<sup>1</sup>, Jericha M. Mateo<sup>1</sup>, Aamir Ahmad<sup>1,2</sup>, Ajaz A. Bhat<sup>3</sup>, Joerg Buddenkotte<sup>1,2,4</sup>, Martin Steinhoff<sup>1,2,4,5,6,7,\*</sup>, Shahab Uddin<sup>1,2,8,\*</sup> 

<sup>1</sup>Translational Research Institute, Academic Health System, Hamad Medical Corporation, 2030 Doha, Qatar

<sup>2</sup>Dermatology Institute, Academic Health System, Hamad Medical Corporation, 2030 Doha, Qatar

<sup>3</sup>Department of Human Genetics-Precision Medicine in Diabetes, Obesity and Cancer Research Program, Sidra Medicine, 26999 Doha, Qatar

<sup>4</sup>Department of Dermatology and Venereology, Rumailah Hospital, Hamad Medical Corporation, 3050 Doha, Qatar

<sup>5</sup>Department of Medicine, Weill Cornell Medicine Qatar, Qatar Foundation-Education City, 24144 Doha, Qatar

<sup>6</sup>Department of Medicine, Weill Cornell Medicine Qatar, New York, NY 10065, USA

<sup>7</sup>College of Medicine, Qatar University, 2713 Doha, Qatar

<sup>8</sup>Laboratory of Animal Research Center, Qatar University, 2713 Doha, Qatar

\*Correspondence: [MSteinhoff@hamad.qa](mailto:MSteinhoff@hamad.qa) (Martin Steinhoff); [Skhan34@hamad.qa](mailto:Skhan34@hamad.qa) (Shahab Uddin)

Academic Editor: Amancio Carnero Moya

Submitted: 10 August 2023 Revised: 30 October 2023 Accepted: 15 November 2023 Published: 23 January 2024

## Abstract

**Background:** The benzophenanthridine Sanguinarine (Sng) is one of the most abundant root alkaloids with a long history of investigation and pharmaceutical applications. The cytotoxicity of Sng against various tumor cells is well-established; however, its antiproliferative and apoptotic potential against the cutaneous squamous cell carcinoma (cSCC) cells remains unknown. In the present study, we investigated the anti-cancer potential of Sng against cSCC cells and elucidated the underlying mechanisms relevant to the drug action. **Methods:** The inhibitory effect of Sng on cSCC cells was evaluated by analyzing cell viability, colony-forming ability and multi-caspase activity. Apoptosis was quantified through Annexin-V/Propidium iodide flow cytometric assay and antagonized by pan-caspase inhibitor z-VAD-FMK. Mitochondrial membrane potential ( $\Delta\Psi_m$ ) dysfunction was analyzed by JC-1 staining, whereas reactive oxygen species (ROS) generation was confirmed by pretreatment with N-acetylcysteine (NAC) and fluorogenic probe-based flow cytometric detection. The expression of cell cycle regulatory proteins, apoptotic proteins and MAPK signaling molecules was determined by Western blotting. Involvement of JNK, p38-MAPK and MEK/ERK in ROS-mediated apoptosis was investigated by pretreatment with SP600125 (JNK inhibitor), SB203580 (p38 inhibitor) and U0126 (ERK1/2 inhibitor), respectively. The stemness-targeting potential of Sng was assessed in tumor cell-derived spheroids. **Results:** Treatment with Sng decreased cell viability and colony formation in primary (A431) and metastatic (A388) cSCC cells in a time- and dose-dependent manner. Sng significantly inhibited cell proliferation by inducing sub-G0/G1 cell-cycle arrest and apoptosis in cSCC cells. Sng evoked ROS generation, intracellular glutathione (GSH) depletion,  $\Delta\Psi_m$  depolarization and the activation of JNK pathway as well as that of caspase-3, -8, -9, and PARP. Antioxidant NAC inhibited ROS production, replenished GSH levels, and abolished apoptosis induced by Sng by downregulating JNK. Pretreatment with z-VAD-FMK inhibited Sng-mediated apoptosis. The pharmacological inhibition of JNK by SP600125 mitigated Sng-induced apoptosis in metastatic cSCC cells. Finally, Sng ablated the stemness of metastatic cSCC cell-derived spheroids. **Conclusion:** Our results indicate that Sng exerts a potent cytotoxic effect against cSCC cells that is underscored by a mechanism involving multiple levels of cooperation, including cell-cycle sub-G0/G1 arrest and apoptosis induction through ROS-dependent activation of the JNK signaling pathway. This study provides insight into the potential therapeutic application of Sng targeting cSCC.

**Keywords:** cutaneous squamous cell carcinoma; Sanguinarine; apoptosis; reactive oxygen species; JNK signaling pathway

## 1. Introduction

Squamous cell carcinoma of the skin or cutaneous squamous cell carcinoma (cSCC) is an epidermal keratinocyte carcinoma that falls under the umbrella of non-melanoma skin cancer (NMSC). It is one of the most frequent neoplasms affecting humans, especially the fair-skinned population, and second only to basal cell carcinoma

in incidence [1]. Several population-based surveys have demonstrated a steady rise in the incidence of cSCC over the last three decades [2–5]. The Australian population has recorded the highest burden of cSCC [6]. cSCC onset generally correlates with cumulative sun exposure (primarily UV-B radiation) and indoor tanning [7], regardless of its multifactorial etiology. Although cSCC is typically benign and indolent, it can present as a spectrum of progressively



advanced stages ranging from precursor actinic keratosis (AK) to invasive and, in rare cases, metastatic cSCC [8,9].

Surgical excision is the mainstay of treatment for common primary cSCC, with a high rate of complete clinical and microscopic resection [10]. However, the management of advanced cSCCs, that encompass unresectable and metastatic disease, has proven challenging causing significant morbidity and mortality. Moreover, the complex molecular landscape and high mutational burden of cSCCs have confounded advances in precision medicine approaches [11]. Nevertheless, recent scientific advances and clinical trials testing new management approaches have significantly improved the National Comprehensive Cancer Network (NCCN) guidelines for cSCC prophylaxis and regional disease treatment with systemic cytotoxic drugs, immune checkpoint inhibitors, and targeted therapies. In addition, many clinical trials have investigated the efficacy of a multimodal approach involving adjuvant systemic therapy, neoadjuvant therapy, or both combined with surgery and/or radiation therapy [12]. Nonetheless, the development of effective drugs against aggressive cSCCs, characterized by high rates of tumor recurrence and the occurrence of secondary primary tumors, is gaining high priority.

In recent years, alternative medicines employing ‘natural agents’, principally phytochemicals, have garnered considerable interest for their potential preventive and therapeutic applications against cSCC [13]. Many preclinical studies have demonstrated the intriguing advantages of these phytochemicals over synthetic chemotherapeutic drugs, attributable to their diverse pharmacological properties, multidimensional targeting, favorable pharmacokinetics and broad safety profiles. For example, topical ingenol mebutate, obtained from the sap of *Euphorbia peplus*, was reported to be an effective and safe therapy for AK [14]. At the molecular level, ingenol mebutate acted as a pleiotropic effector, inducing cell death and manipulating immune-mediated responses [15]. Curcumin, a broad-spectrum phenolic compound extracted from turmeric (*Curcuma longa*) rhizome, has also been shown to inhibit cSCC growth and tumor progression *in vivo* by inhibiting the mTOR pathway [16].

Sanguinarine (Sng), derived from plants such as *Sanguinaria canadensis* and *Macleaya cordata*, belongs to the group of benzylisoquinolines and has been classified as an alkaloid antibiotic and botanical antifungal agent [17]. The anti-cancer potential of Sng has also been established both *in vitro* and *in vivo* against various human malignancies, such as colorectal cancer [18], head and neck cancer [19] and drug-resistant non-small-cell lung cancer [20]. Sng has been shown to induce apoptosis (extrinsic and intrinsic) in cancer cells through several mechanisms, including reactive oxygen species (ROS) generation and activation of c-Jun-N-terminal kinase (JNK) and nuclear factor-kappa B (NF- $\kappa$ B) signaling pathways [19–22]. In addition, Sng has been identified as a potent anti-angiogenic phytochem-

ical because it inhibits vascular endothelial growth factor (VEGF)-induced angiogenesis [23]. In relation to skin conditions, Reagan-Shaw *et al.* [24] demonstrated the photoprotective effects of Sng against UV-B-induced damage in human HaCaT skin keratinocytes *in vitro*. Extrapolating the *in vitro* results *in vivo*, the same group demonstrated the chemopreventive potential of Sng against UV-B-mediated damage in a hairless mouse model [25].

In the present study, we adopted an *in vitro* approach to investigate Sng’s anti-cancer and therapeutic potential in cSCC. Herein, we provide experimental evidence of Sng-mediated suppression of cSCC cell growth and stemness potential via apoptosis through ROS-dependent activation of the JNK signaling pathway.

## 2. Materials and Methods

Human cSCC epithelial cells A431 (primary; source: male) and A388 (metastatic; source: female) were obtained from American Type Culture Collection (ATCC, Manassas, VA, USA). The cell lines were routinely tested to ensure they were free of microbial contamination. Cells were cultured in DMEM (Gibco, ThermoFisher Scientific, MA, USA) supplemented with 10% (*v/v*) fetal bovine serum (FBS) and 1% (*v/v*) penicillin-streptomycin (Gibco, ThermoFisher Scientific, MA, USA) and maintained in a humidified 5% CO<sub>2</sub> atmosphere at 37 °C. All the treatments were performed in 5% DMEM.

All the cell lines utilized in this study were procured from the ATCC, accompanied by a Certificate of Analysis confirming their authentication through STR profiling and their mycoplasma-free status. Upon receipt, the cell lines were immediately thawed and cultured according to standard protocols in a humidified incubator maintained at 37 °C and 5% CO<sub>2</sub>. The cell lines were continuously monitored for consistency in growth, morphology, and behavior throughout the experimental period.

### 2.1 Cell Viability Assessment Using CCK-8

The *in vitro* cellular cytotoxicity of Sng alone and in combination with inhibitors against cSCC cells was evaluated using the Cell Counting Kit-8 (CCK-8) assay, as described previously [26]. Firstly, Sng (Sigma-Aldrich, St. Louis, MO, USA) was dissolved in DMSO (Sigma-Aldrich, St. Louis, MO, USA) to make a stock solution and further diluted with the corresponding culture fluid to make a series of drug solutions. cSCC (10<sup>4</sup>) cells in the exponential phase were seeded into each well of a 96-well plate. Following incubation at 37 °C under a humidified atmosphere of 5% CO<sub>2</sub> for 24 h, the cells were exposed to a series of concentrations of Sng (0.5, 1, 2, 4, 8, and 16  $\mu$ M) and in combination with pharmacological inhibitors. Finally, 10  $\mu$ L of CCK-8 reagent (Sigma-Aldrich, St. Louis, MO, USA) was added to each well according to the manufacturer’s protocol, and the spectrophotometric absorbance (optical density [OD]) was measured at 450 nm using a multifunction mi-

croplate reader (Tecan Bio Tek Instruments Inc., Morgan Hill, CA, USA). The percentage of cell viability was calculated as follows: OD of the experimental sample/OD of the control sample  $\times$  100.

## 2.2 Impedance Measurement by Real-Time Cell Analysis (RTCA)

The time- and dose-dependent cellular response profiles of Sng treatment were measured using the xCELLigence Real-Time Cell Analysis high-throughput detection platform. After setting up the program, 50  $\mu$ L of cell culture medium was added to each well of an E-plate 16 (ACEA Biosciences, San Diego, CA, USA). After equilibration at 37 °C for 30 min, the E-plates were inserted into the xCELLigence RTCA station (ACEA Biosciences, San Diego, CA, USA) to check for appropriate electrical connections and gather the background impedance of the cell culture medium. A431 and A388 cells were resuspended in cell culture medium, seeded at the required cell density into each well of the E-plate, and incubated for 24 h at 37 °C with 5% CO<sub>2</sub> in the RTCA cradle. Following incubation, the culture medium was removed, and the cells were treated with escalating concentrations (1, 2, 4, 8 and 16  $\mu$ M) of Sng. After adding Sng, the impedance signal (expressed as the cell index readout) was recorded every 15 min for approximately 250 h. The analysis and interpretation of the impedance pattern over time were performed using RTCA software (ACEA Biosciences, San Diego, CA, USA).

## 2.3 Evaluation of Cell Viability by Trypan Blue Assay

The cellular response to pharmacological inhibitors, with or without Sng, was assessed via the trypan blue dye exclusion assay [27]. Briefly, A388 cells were seeded in 60-mm culture plates and maintained for 24 h in complete DMEM medium. Post incubation, cells were pretreated with SB203580 (a p38 inhibitor; 20  $\mu$ M) or U0126 (an ERK1/2 inhibitor; 20  $\mu$ M) for 2 h followed by the treatment with Sng (4  $\mu$ M) for 6 h. Following treatment, the cells were harvested, centrifuged, and resuspended in 1 mL PBS. Cells were then stained with 0.4% trypan blue solution (1:1; Sigma-Aldrich, St. Louis, MO, USA), and 10  $\mu$ L of cell suspension was applied to the edge of the dual-chamber cell counting slide (Bio-Rad, Hercules, CA, USA). Finally, the slide was inserted into the TC20™ automated cell counter (Bio-Rad, Hercules, CA, USA), and the cell viability was estimated as the percentage of live cells in the sample via trypan blue exclusion.

## 2.4 Live and Dead Assay

The LIVE/DEAD® Viability Kit (Life Technologies Corporation, Carlsbad, CA, USA) was used according to the manufacturer's instructions and as previously described [28] to visualize the distribution of viable and non-viable A431 and A388 cells 24 h post-treatment with Sng alone and in combination with inhibitors. Briefly, A388 and

A431 cells were seeded at a density of  $1 \times 10^6$  cells per well in a 6-well plate and subjected to a 24 h treatment with varying concentrations of Sng alone (2, 4, and 8  $\mu$ M), in combination with N-acetylcysteine (NAC; 10 mM; Sigma-Aldrich, St. Louis, MO, USA) as well as z-VAD-FMK (50  $\mu$ M; Calbiochem, San Diego, CA, USA). Cells were then stained with the live/dead stain prepared by diluting 20  $\mu$ L of ethidium homodimer-1 (EthD-1; final concentration: 4  $\mu$ M) and 5  $\mu$ L calcein AM (final concentration: 2  $\mu$ M) in 10 mL of PBS. Green and red fluorescent signals from calcein-AM and EthD-1, respectively, were detected using the EVOS FLc cell imaging system (Invitrogen, Thermo Fisher Scientific, MA, USA).

## 2.5 Colony-Forming Assay

The colony-forming assay was performed as described previously [29] to evaluate the proliferative and colony-forming abilities of A388 and A431 cells treated with Sng alone and in combination with inhibitors. Following optimization of the number of cells required to obtain the best size and distribution of colonies, A431 and A388 cells were seeded at a density of  $10^4$  cells/well in a 6-well plate. After 24 h of incubation, cells were treated with varying concentrations of Sng alone and in combination with inhibitors (NAC, 10 mM; z-VAD-FMK, 50  $\mu$ M) and incubated for 7 days in a humidified atmosphere at 37 °C with 5% CO<sub>2</sub>. After obtaining sufficiently sized colonies, cells were fixed with 10% (w/v) formaldehyde and stained with 0.1% (w/v) crystal violet solution for 30 min at room temperature. The staining solution was then carefully drained, and each well was washed with water until the excess dye was removed. Finally, colonies were visualized at 4 $\times$  magnification using an EVOS FLc cell imaging system (Invitrogen, Thermo Fisher Scientific, MA, USA).

## 2.6 Apoptosis Assay by Annexin V/Propidium Iodide (PI) Dual Staining

The quantification of apoptosis and necrosis after treatment with Sng alone and in combination with inhibitors (NAC, 10 mM; z-VAD-FMK, 50  $\mu$ M; and SP600125, 30  $\mu$ M) was performed using conventional Annexin V-FITC and Propidium iodide (PI) staining (Annexin V-FITC apoptosis detection kit, BD Biosciences, San Jose, CA, USA) followed by flow cytometric analysis. Approximately  $1 \times 10^6$  cells subjected to various treatments were centrifuged at 1500 rpm for 5 min at 4 °C before being washed in 1 mL PBS, centrifuged again, and diluted in  $1 \times$  annexin binding buffer. Annexin V-FITC (10  $\mu$ L) and PI (5  $\mu$ L) were added to the suspension, and the tubes were incubated for 20 min in the dark at room temperature. Different cell populations were selected and viable and apoptotic cells were sorted by fluorescence-activated cell sorting using flow cytometry (BD LSR Fortessa cell analyzer; BD Biosciences, San Jose, CA, USA). The cells were identified and quantified as live (Annexin FITC<sup>-ve</sup>/PI<sup>-ve</sup>), early or primary

apoptotic (Annexin FITC<sup>+</sup>/PI<sup>-</sup>), late apoptotic (Annexin FITC<sup>+</sup>/PI<sup>+</sup>), and necrotic (Annexin FITC<sup>-</sup>/PI<sup>+</sup>). Debris and cell aggregates were excluded from the analysis.

### 2.7 Flow Cytometric Measurement of Intracellular Mitochondrial Membrane Potential ( $\Delta\Psi_m$ )

To evaluate the capacity of Sng to modulate the mitochondrial membrane potential ( $\Delta\Psi_m$ ) in cSCC cells, the mitochondria-specific ratiometric fluorescent dye tetraethylbenzimidazolylcarbocyanine iodide (JC-1) was used. Following 24 h treatment with Sng and in combination with inhibitors (NAC, 10 mM; and z-VAD-FMK, 50  $\mu$ M), A388 and A431 cells were harvested, washed, resuspended in 1 mL PBS, and stained with JC-1 staining solution (BD Biosciences, San Jose, CA, USA) in the dark. Cells maintained on ice were then immediately analyzed for  $\Delta\Psi_m$  using flow cytometry (BD LSR Fortessa analyzer, BD Biosciences, San Jose, CA, USA).

### 2.8 Flow Cytometric Analysis of Activated Caspase-3 and Cleaved Poly (ADP-ribose) Polymerase (PARP)

First, A388 and A431 cells were treated with Sng alone or in combination with z-VAD-FMK (50  $\mu$ M) for 24 h. After treatment, cells were harvested, washed twice in PBS, and centrifuged. The cells were then fixed and permeabilized using a BD Cytofix/Cytoperm Plus Fixation kit (BD Biosciences, San Jose, CA, USA) according to the manufacturer's protocol. Approximately  $1 \times 10^6$  cells were stained with 5  $\mu$ L of BV605-tagged active caspase-3 and 5  $\mu$ L of AF647-tagged cleaved PARP for 30 min and analyzed using flow cytometry (BD LSR Fortessa analyzer, BD Biosciences, USA).

### 2.9 Flow Cytometric Detection of ROS

To investigate Sng-induced oxidative stress, we pursued the generation of ROS in A388 and A431 cells treated with Sng alone or in combination with NAC (10 mM) or z-VAD-FMK (50  $\mu$ M). 24 h post-treatment, the cells were harvested, washed using Hanks' balanced salt solution (HBSS), and stained with CellROX<sup>TM</sup> Green Reagent (10  $\mu$ M; to detect intracellular ROS) and MitoSOX Red reagent (5  $\mu$ M; to detect mitochondrial superoxide) for 30 min at 37 °C. ROS levels were quantified using flow cytometry (BD LSR Fortessa analyzer, BD Biosciences, USA).

### 2.10 Quantification of DNA Double-Strand Breaks (DSBs)

Sng-induced DNA double-strand breaks (DSBs) were analyzed by detecting phosphorylated histone H2AX Ser139 (p-H2AX<sup>Ser139</sup>) as previously described [30]. A431 and A388 cells were treated for 24 h with various concentrations of Sng alone or in combination with z-VAD-FMK (50  $\mu$ M). After incubation, the cells were fixed and permeabilized using the BD Cytofix/Cytoperm plus fixation and permeabilization solution kit according to the manufacturer's protocol. Approximately  $1 \times 10^6$  cells were stained with

5  $\mu$ L f BV421 Mouse Anti-H2AX (pS139) antibody (BD Biosciences, San Jose, CA, USA) for 30 min at room temperature. Phosphorylated histone H2AX levels were then detected by flow cytometry using a BD LSR Fortessa analyzer (BD Biosciences, USA).

### 2.11 Flow Cytometric Analysis of Cell-Cycle Distribution

The effect of Sng on cell cycle distribution was analyzed as previously described [26]. A388 and A431 cells were seeded in 100-mm culture dishes and treated with gradient concentrations of Sng alone and in combination with NAC (10 mM) or z-VAD-FMK (50  $\mu$ M) for 24 h. After treatment, cells were harvested, centrifuged, and fixed in ethanol (70%) for 2 h. For analysis, cells were resuspended in PBS, incubated with RNase A solution (0.04  $\mu$ g/mL) for 30 min at 37 °C, and then treated with PI DNA cell-cycle stain (40  $\mu$ g/ $\mu$ L) for 30 min at 4 °C. By gating the forward and side scatter profiles of the samples, doublets, disintegrated nuclei, and other cell debris were excluded from the analysis. The gates were uniformly maintained across all the samples in each cycle. After that, the relative DNA content was determined, and the percentages of cells in the sub-G0/G1, G0/G1, S, and G2/M phases were quantified by flow cytometry (BD LSR Fortessa analyzer, BD Biosciences, USA) based on the amount of PI fluorescence.

### 2.12 Tumor Cell Spheroid Culture

Tumor-derived spheroids/tumorspheres from A388 cells were generated in non-adsorbent, ultra-low attachment, 6-well plates (Corning, USA). The two-dimensional cell culture was maintained for 24 h under standard culture conditions (37 °C with 5% CO<sub>2</sub>) in complete DMEM. After the two-dimensional cell culture was harvested, the cells were dissociated into a single-cell suspension through enzymatic digestion (trypsin). Five thousand cells were then added to each well of a 6-well plate and grown in complete cancer stem cell medium (3D Tumorsphere Medium XF, Promo Cell, Germany, C-28070). The plates were then placed in a humidified incubator at 37 °C with 5% CO<sub>2</sub> until spheroids with 400–500  $\mu$ m diameters were formed. The spheroids were treated with Sng alone or in combination with NAC (10 mM) or SP600125 (30  $\mu$ M) for 7 days. Spheroid formation was monitored on days 0, 3, and 7 using the EVOS FLc cell imaging system (Invitrogen, Thermo Fisher Scientific) at 10 $\times$  and 20 $\times$  magnification.

### 2.13 Protein Extraction and Immunoblotting

Following cell lysis with a 2X Laemmli sample buffer (Bio-Rad, Hercules, CA, USA), the total protein from cells was extracted and quantified using a Nanodrop ND-100 spectrophotometer (Thermo Fisher Scientific). Approximately 30–100  $\mu$ g of protein from each sample was loaded and resolved by SDS-PAGE (10–12%), transferred to a polyvinylidene difluoride (PVDF) membrane, and blotted with primary antibodies against p-p38

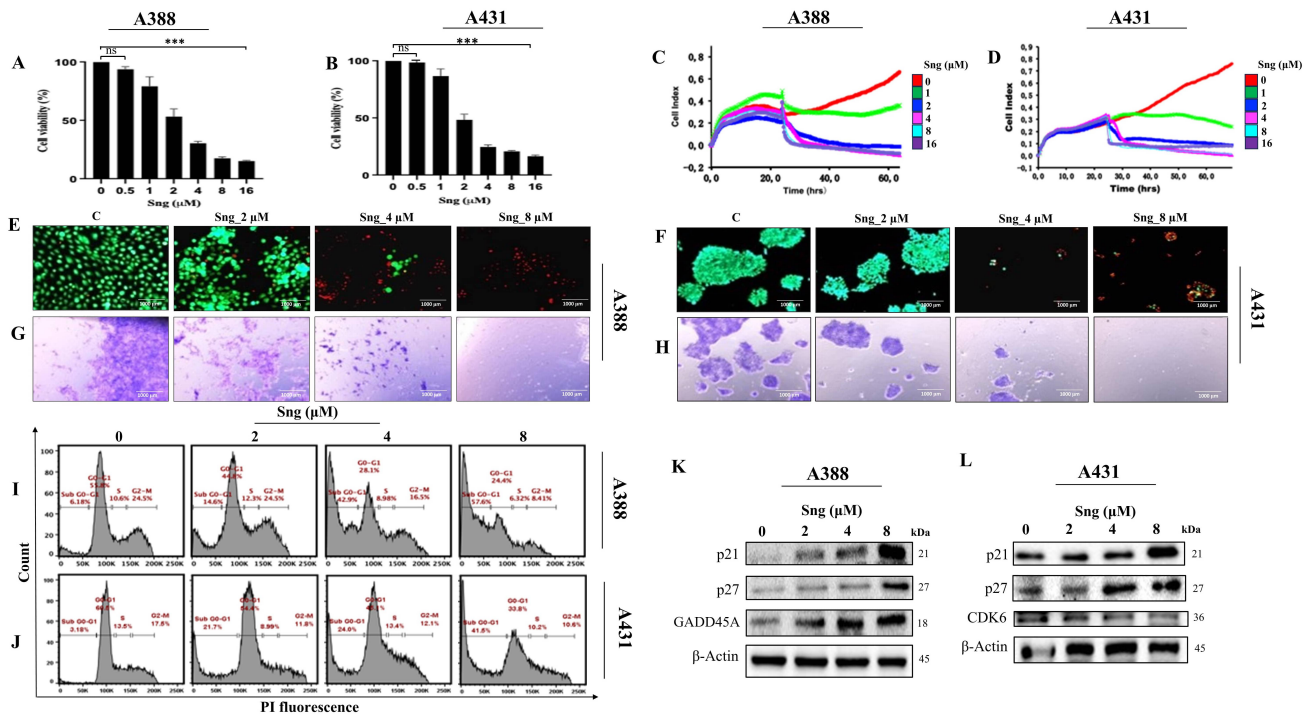


**Fig. 1. Sanguinarine (Sng) inhibits proliferation, impairs viability, and induces cell-cycle perturbations in cutaneous squamous cell carcinoma (cSCC) cells.** (A–D) Metastatic (A388) and primary (A431) cSCC cells were treated with various concentrations of Sng (0.5–16 μM) for 24 h. The viability of the cells was determined by the CCK-8 assay (A,B) while the Real-Time Cell Analysis (RTCA) system was used to record the cell growth curves in response to different concentrations of Sng (1–16 μM) (C,D) Data represented as mean ± SD from three independent experiments. ns: not significant, \*\*\* $p < 0.001$ ; one-way ANOVA followed by Tukey analysis. (E,F) The distribution of live (indicated by green fluorescence) and dead (indicated by red fluorescence) A388 and A431 cells following Sng treatment (2 μM, 4 μM, and 8 μM) for 24 h (magnification 4×; scale bar: 1000 μm). (G,H) Colony-forming efficiency of A388 and A431 cells exposed to indicated concentrations of Sng (magnification 4×; scale bar: 1000 μm). (I,J) Frequency histograms from flow cytometry showing the regulatory effect of Sng on cell-cycle distribution in A388 and A431 cells exposed to indicated concentrations of Sng for 24 h. Each histogram shows the quantified percentages of DNA content and cell-cycle distribution for sub-G0/G1, G0/G1, S, and G2/M phases. (K,L) Expression profile of cell-cycle regulatory proteins in A388 and A431 cells treated with increasing concentrations of Sng for 6 h. SD, standard deviation; CCK-8, Cell Counting Kit-8; ANOVA, analysis of variance.

(Thr180/Tyr182), p38, p-p44/42 (Thr202/Tyr204), p44/42, p27, p21, CDK6, caspase-3, caspase-9, cleaved caspase-8, PARP, BH3 interacting-domain death agonist (Bid), growth arrest-and DNA damage-induced 45 A (GADD45A), and p-H2AX<sup>Ser139</sup> (Cell Signaling Technologies, Danvers, MA, USA) as well as p-JNK (Thr183/Tyr185), JNK, and Bcl-2-associated X protein (Bax) (Santa Cruz Biotechnology Inc., Dallas, TX, USA). After incubation with the corresponding secondary antibodies, the protein bands were detected using a Chemi-Doc System with an ECL substrate (Bio-Rad, Hercules, CA, USA). Internal controls such as GAPDH (Cell Signaling Technologies, Danvers, MA, USA), β-Actin, α-tubulin, and HSP60 (Santa Cruz Biotechnology Inc., Dallas, TX, USA) were used.

#### 2.14 Statistical Analysis

The statistical significance between the treated and untreated samples was analyzed by one-way ANOVA followed by Tukey's multiple comparison test using GraphPad

Prism. All error bars represent the mean ± standard deviation (SD) of three independent experiments.  $p$  values < 0.001 were considered statistically significant.

### 3. Results

#### 3.1 Sanguinarine Inhibits the Growth and Proliferation of cSCC Cells

Several toxicological studies have demonstrated the anti-cancer potential of Sng in both *in vitro* and *in vivo* tumor models [31–35]. To obtain an accurate assessment of the Sng dose-response in cSCC cells, cell viability was assessed upon screening with escalating concentrations of Sng (0.5–16 μM) for 24 h. Sng began to show a response at 2 μM, evident from the significant decrease in the number of viable cells in both A388 and A431 cells (Fig. 1A,B). The RTCA system was also used to evaluate the cytotoxic actions of Sng. Being a high-throughput and quantitative technique, RTCA enables continuous, label-free and real-

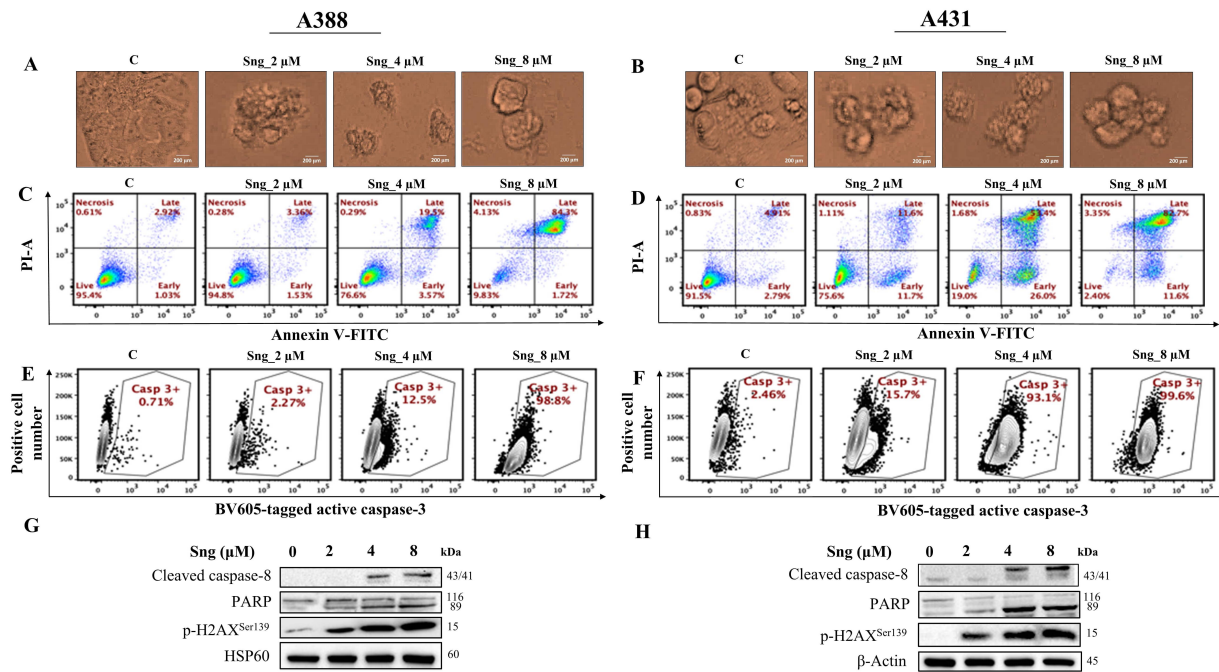


**Fig. 2. Sanguinarine induces apoptosis in cSCC cells.** (A,B) Microscopic images of cSCC cells showing morphological abnormalities induced by Sng (2  $\mu$ M, 4  $\mu$ M, and 8  $\mu$ M) (magnification 20 $\times$ ; scale bar: 200  $\mu$ m). (C,D) Scatter plots presenting the kinetics of apoptosis in A388 and A431 cells treated with indicated concentrations of Sng. The percentages of apoptotic, necrotic and live cells were determined and analyzed by Annexin V-FITC/PI staining using flow cytometry after 24 h. The plot depicts segregation into four quadrants: the lower-left quadrant representing viable cells (Annexin V-FITC<sup>ve</sup>/PI<sup>ve</sup>); the lower-right quadrant representing cells that are in early apoptosis (Annexin V-FITC<sup>ve</sup>/PI<sup>ve</sup>); the upper-left quadrant representing cells that are in necrotic phase (Annexin V-FITC<sup>ve</sup>/PI<sup>ve</sup>); and the upper-right quadrant representing cells that are in late apoptosis (Annexin V-FITC<sup>ve</sup>/PI<sup>ve</sup>). (E,F) Scatter plots depicting the activity of caspase-3 in A388 and A431 cells treated with the indicated concentrations of Sng. A388 and A431 cells were treated with indicated concentrations of Sng for 24 h and then assessed for the activity of caspase-3 tagged with BV605 dye using flow cytometry. (G,H) Western blot analysis of cleaved caspase-8, Poly (ADP-ribose) Polymerase (PARP), and phosphorylated histone H2AX Ser139 (p-H2AX<sup>Ser139</sup>) in A388 and A431 cells treated with indicated concentrations of Sng for 6 h. FITC, fluorescein isothiocyanate; PI, Propidium Iodide.

time monitoring of dose-dependent cellular responses such as cell proliferation and morphological alterations [36]. Dynamic real-time monitoring of cSCC cells treated with Sng confirmed the antiproliferative effect of the compound, and results were comparable to those obtained from the CCK-8 assay (Fig. 1C,D). Because the reduction in the number of viable cells obtained from the CCK-8 assay could have been caused either by cytotoxicity or inhibited cell proliferation, we performed a LIVE/DEAD<sup>®</sup> cell viability assay, which detects live and dead cells from the fluorescence emitted by calcein AM and EthD-1, respectively. The live/dead assay also confirmed the effective cytotoxicity exerted by Sng on A388 and A431 cells, as evidenced by the significant reduction in the number of viable cells (reflected by the green fluorescent signal) after Sng treatment compared to the control group. Moreover, it provided proof of apoptosis, as indicated by an increase in the relative number of dead cells (reflected by the red fluorescent signal) (Fig. 1E,F). To assess the effect of Sng on reproductive cell survival and growth *in vitro*, we used a conventional 2D clonogenic or

colony formation assay. Fig. 1G,H show whole-well images of colony formation across all treatment groups and reflect the capacity of Sng to influence and antagonize the extent of clonogenic growth (reflected by the number and size of tumor cell colonies) of both primary and metastatic cSCC cells.

In addition to the drug dose-response, it is crucial to quantitatively assess the growth-inhibitory effect of the drug as a function of exposure time. To track the cellular response to Sng across time, A388 and A431 cells were exposed to 2  $\mu$ M Sng at different time points (0–48 h) and subjected to toxicity and viability measurements. Time-dependent analysis of cellular response from 0 to 48 h indicated a decline in cell viability (Supplementary Fig. 1a,b), as well as morphological and biochemical changes consistent with apoptosis, including activation of caspase-3, -8 and DNA fragmentation (Supplementary Fig. 1c–f). These results implied the dose- and time-dependent cytotoxic effects of Sng in cSCC cells.

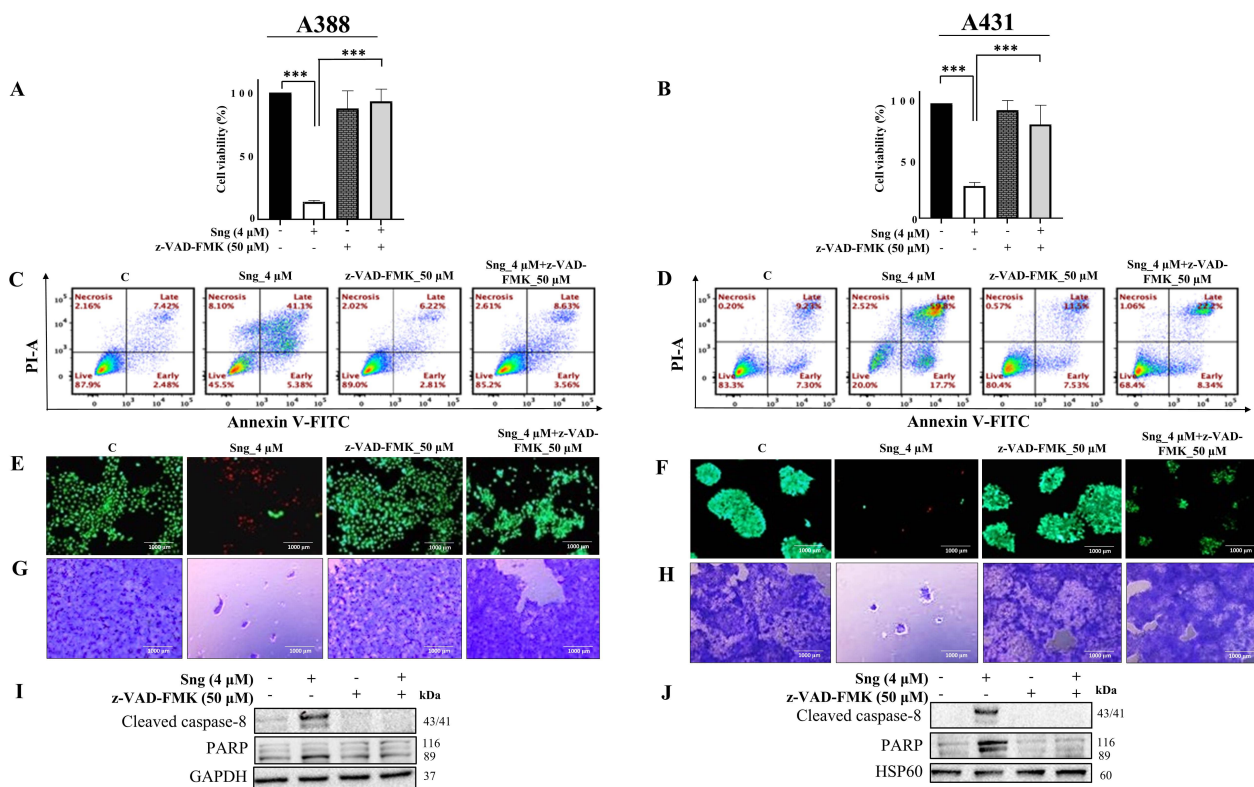


**Fig. 3. Sanguinarine induces caspase-mediated apoptosis in cSCC cells.** (A,B) Pretreatment with the general caspase inhibitor z-VAD-FMK restores cell viability in A388 and A431 cells following exposure to Sng. A388 and A431 cells were pretreated with 50 μM z-VAD-FMK for 1 h before being challenged with 4 μM Sng. Cell viability was determined by CCK-8 analysis. Data presented as the mean ± SD from three independent experiments. \*\*\* $p < 0.001$  compared with the Sng-treated group; one-way ANOVA followed by Tukey analysis. (C,D) Scatter plots presenting the kinetics of apoptosis in cells co-treated with z-VAD-FMK and Sng. A388 and A431 cells were pretreated with 50 μM z-VAD-FMK for 1 h before being challenged with 4 μM Sng for 24 h. (E,F) Representative fluorescence staining depicting the distribution of live (indicated by green fluorescence) and dead (indicated by red fluorescence) A388 and A431 cells following treatment with z-VAD-FMK (50 μM), either alone or in combination with Sng (4 μM) for 24 h (magnification 4×; scale bar: 1000 μm). (G,H) Colony-forming efficiency of A388 and A431 cells co-treated with z-VAD-FMK (50 μM) and Sng (4 μM) for 24 h (magnification 4×; scale bar: 1000 μm). (I,J) Western blot analysis of cleaved caspase-8 and PARP expression in A388 and A431 cells pretreated with z-VAD-FMK (50 μM) for 1 h followed by treatment with Sng (4 μM) for 6 h.

Concerning the cytostatic assessment of Sng via fluorescent PI-based quantification of cell-cycle distribution, we determined that Sng alters the cell cycle machinery by markedly increasing the accumulation of the pro-apoptotic sub-G0/G1 fraction in both A431 and A388 cells in a concentration-dependent manner (Fig. 1I,J). Subsequently, western blot analysis was performed to delineate the molecular mechanisms underlying Sng-induced cell-cycle arrest. The analysis showed that Sng modulates cell cycle regulatory proteins, manifested by the upregulated expression of cyclin-dependent kinase inhibitors p21<sup>WAF1/Cip1</sup> and p27<sup>Kip1</sup> and the downregulated expression of CDK6. Notably, Sng induced a concentration-dependent increase in the expression of GADD45A in metastatic A388 cells (Fig. 1K,L). According to these results, Sng exerts its antiproliferative effects by modulating checkpoints at the sub-G0/G1 phase of the cell cycle and inducing sub-G0/G1 phase arrest in cSCC cells.

### 3.2 Sanguinarine Prompts Caspase-Mediated Apoptosis in cSCC Cells

Focusing on the mechanistic aspects of cytotoxicity induced by Sng, we sought to unveil and characterize the major regulated cell death (RCD) modality [37] initiated by perturbations in the intracellular or extracellular microenvironments of cSCC cells. Since apoptosis has been reported to be the most profound RCD program triggered by Sng [26,38], we assessed concentration-dependent morphological response that is characteristic of apoptosis in cSCC cells following exposure to Sng for 24 h. As shown in Fig. 2A,B, the morphological hallmarks of apoptosis, including cell shrinkage, membrane blebbing, and membrane-bound apoptotic bodies, were observed. To quantify apoptotic rates and segregate the apoptotic population, cSCC cells were subjected to Annexin V/PI staining. As shown in Fig. 2C,D, the majority of the Sng-treated cell population was in a late apoptotic state, although there

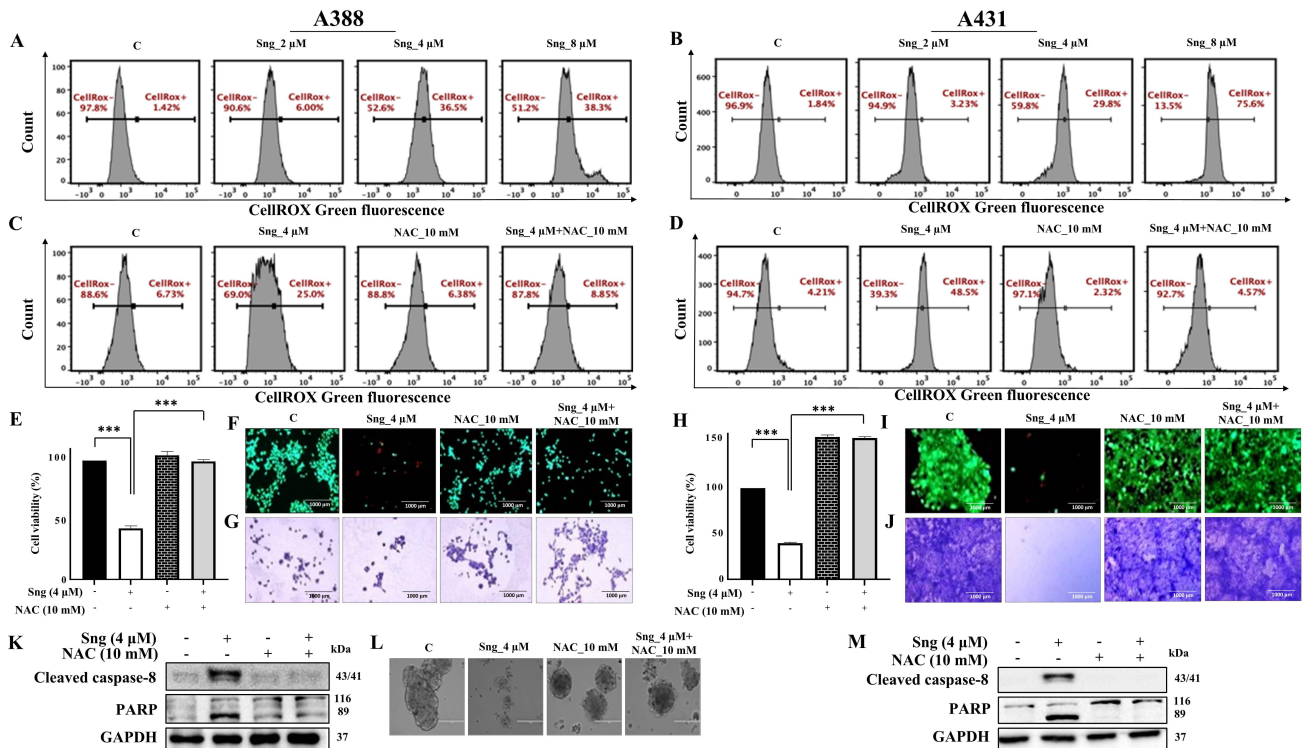


**Fig. 4. Sanguinarine induces reactive oxygen species (ROS)-dependent apoptosis in cSCC cells.** (A,B) Frequency histograms showing the generation of intracellular ROS in A388 and A431 cells treated with increasing concentrations of Sng for 24 h. (C,D) Frequency histograms showing the effect on intracellular ROS in A388 and A431 cells following pretreatment with N-acetylcysteine (NAC) (10 mM) and then by Sng (4 μM) for 24 h. (E,H) Pretreatment with the ROS scavenger NAC restores cell viability in A388 and A431 cells following exposure to Sng. A388 and A431 cells were pretreated with 10 mM NAC for 1 h before being challenged with 4 μM Sng. Cell viability was determined by CCK-8 analysis. Data presented as the mean ± SD from three independent experiments. \*\*\* $p < 0.001$  compared with the Sng-treated group; one-way ANOVA followed by Tukey analysis. (F,I) Representative fluorescence staining depicting the distribution of live (indicated by green fluorescence) and dead (indicated by red fluorescence) A388 and A431 cells following treatment with NAC (10 mM), either alone or in combination with Sng (4 μM) for 24 h (magnification 4×; scale bar: 1000 μm). (G,J) Colony-forming efficiency of A388 and A431 cells co-treated with NAC (10 mM) and Sng (4 μM) (magnification 4×; scale bar: 1000 μm). (K,M) Western blot analysis of cleaved caspase-8 and PARP in A388 and A431 cells co-treated with NAC (10 mM) and Sng (4 μM) for 6 h. (L) Inhibition of dissolution and apoptosis in A388 spheroids on pretreatment with NAC (magnification 20×; scale bar: 200 μm).

was a significant increase in the percentages of both early and late apoptotic A388 and A431 cells associated with increasing concentrations of Sng. Induction of apoptotic cell death typically occurs via two major pathways: an extrinsic death receptor pathway and an intrinsic/mitochondrial pathway. Each of these pathways requires specific initiating stimuli to activate specific initiator caspases [39] and, in turn, executioner caspase-3. To ascertain whether the extrinsic pathway was associated with Sng-induced apoptosis, we assessed the expression of caspase-8 and caspase-3 in A388 and A431 cells treated with increasing concentrations of Sng. Treatment with Sng increased the expression of both caspase-3 (Fig. 2E,F) and cleaved caspase-8 (Fig. 2G,H) in the A388 and A431 cells in a concentration-dependent manner. Given that PARP is the preferred cellular substrate for caspases, we analyzed the cleavage of PARP in response to caspase-3 activation induced by Sng.

As shown in Fig. 2G,H, and **Supplementary Fig. 2a,b**, there was an obvious increase in the activity of PARP, represented by its cleaved form, in both A388 and A431 cells exposed to increasing concentrations of Sng. DNA fragmentation is a biochemical hallmark of apoptosis, which can be detected through the phosphorylation status and foci formation of H2AX in cells [40]. Exposure to Sng triggered a concentration-dependent increase in Ser139 phosphorylation of H2AX in A388 and A431 cells, indicating the significant genotoxic effect of Sng (Fig. 2G,H). These findings suggest the execution of a caspase-dependent extrinsic signaling pathway following the cell death stimulus generated by Sng.

To substantiate the role of caspases in Sng-induced cellular apoptosis, A388 and A431 cells were preincubated with the pan-caspase inhibitor z-VAD-FMK (50 μM), followed by treatment with Sng (4 μM). z-VAD-FMK is a



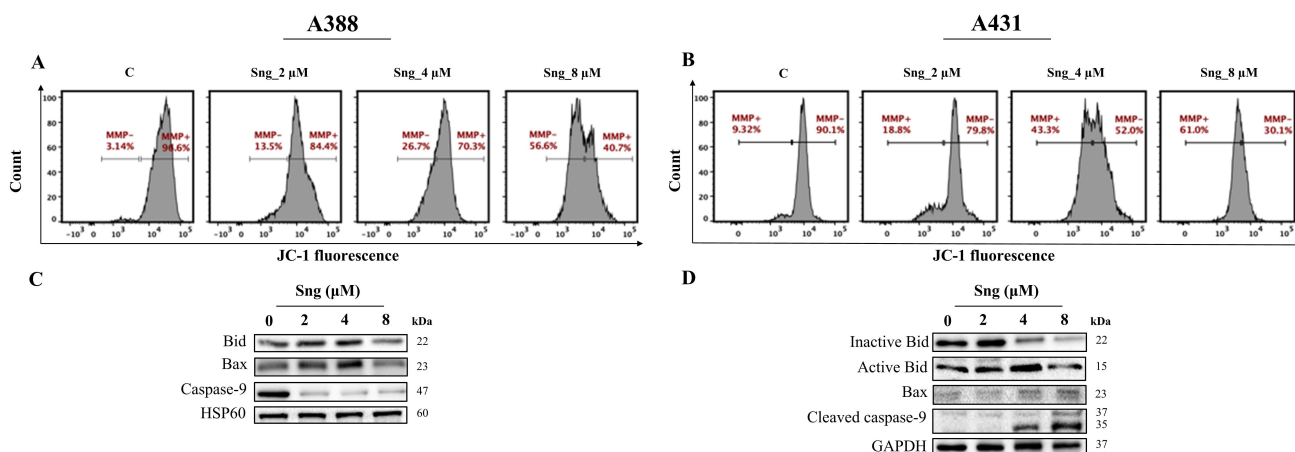


**Fig. 5. Disruption of mitochondrial membrane potential in response to Sanguinarine in cSCC cells.** (A,B) Distribution plots representing the percentage of cells exhibiting loss of  $\Delta\Psi_m$  after exposure to indicated concentrations of Sng in A388 and A431 cells. (C,D) Western blot analysis of BH3 interacting-domain death agonist (Bid), Bcl-2-associated X protein (Bax), and caspase-9 expression in A388 and A431 cells subsequent to the loss of  $\Delta\Psi_m$  induced by Sng.

cell-permeable, irreversible fluoromethyl ketone (FMK)-derivatized peptide that acts as an efficient caspase inhibitor [41]. Applying z-VAD-FMK significantly restored the viability of the Sng-treated A388 and A431 cells (Fig. 3A,B). Evaluation of specific cell fractions by Annexin V/PI staining revealed that preventing the cleavage of caspases with z-VAD-FMK remarkably attenuated the accumulation of apoptotic cells relative to cells treated with Sng alone (Fig. 3C,D). The percentage of apoptotic (early and late) cells appeared as a readout of enhanced apoptosis in Sng-treated cells but was minimally detectable in z-VAD-FMK and Sng co-treated cells. Similarly, the Live/Dead assay also revealed an increase in the density of live cells in the z-VAD-FMK-treated group (Fig. 3E,F), corroborating the flow cytometry results. The clonogenic abilities of A388 and A431 cells were also restored upon pretreatment with z-VAD-FMK (Fig. 3G,H). Furthermore, co-treatment of cells with z-VAD-FMK and Sng significantly antagonized the expression of Sng-induced cleaved caspase-8 and PARP (Fig. 3I,J). These findings suggest that Sng induces caspase-dependent apoptosis in cSCC cells.

Delving deeper into the activity of z-VAD-FMK, we assessed whether z-VAD-FMK can reverse Sng-induced cell-cycle defects and found that z-VAD-FMK prevented the accumulation of sub-G0/G1 fraction in A388 cells (Supplementary Fig. 3e). Because Sng-treated cells expressed active caspase-3, we sought to determine its expression in response to pretreatment with z-VAD-FMK. z-VAD-FMK reduced the expression of active caspase-3 compared to that in the Sng-treated group (Supplementary Fig. 3e). Moreover, we quantified p-H2AX<sup>Ser139</sup> levels and, thus, DNA damage in cells that were co-treated with z-VAD-FMK and Sng, considering that p-H2AX levels were distinctly elevated upon Sng treatment. Quantification of p-H2AX<sup>Ser139</sup> levels by flow cytometry showed that the cell

fraction from the co-treated group displayed p-H2AX levels comparable to those in the control group (Supplementary Fig. 3f).

### 3.3 Sanguinarine Mediates Apoptosis via Intracellular and Mitochondrial ROS Production in cSCC Cells

ROS, a class of highly reactive molecules, are critical regulators of apoptosis. Considering the bidirectional nature of ROS [42], we determined the ability of Sng to manipulate levels of ROS in cSCC cells. Using CellROX and MITOSOX fluorogenic probes, we showed that Sng markedly increased intracellular (Fig. 4A,B) and mitochondrial (Supplementary Fig. 2c,d) ROS production in a concentration-dependent manner in both A388 and A431 cells. This ROS production was blocked by NAC (10 mM), a universal cytoprotective antioxidant that serves as a ROS scavenger and precursor of glutathione (GSH) synthesis in Sng-treated A388 (Fig. 4C; Supplementary Fig. 4a) and A431 cells (Fig. 4D). NAC also restored GSH levels (Supplementary Fig. 4d) that were elevated in A388 and A431 cells exposed to Sng (Supplementary Fig. 2e,f).

Next, we investigated the role of ROS in the regulation of Sng-induced apoptosis. Pretreatment with NAC remarkably preserved cell viability and abrogated cytotoxicity in Sng-treated A388 (Fig. 4E,F) and A431 cells (Fig. 4H,I). The clonogenic assay in Fig. 4G,J further suggested that NAC restored cell survival and clonal expansion of A388 and A431 cells compared to cells treated with Sng alone. Furthermore, applying NAC decreased the sub-G0/G1 population (Supplementary Fig. 4b) of A388 cells. To determine whether ROS production precedes caspase-dependent apoptosis in cSCC cells, we determined cleaved caspase-8 and PARP expression levels in A388 and A431 cells cotreated with NAC and Sng. The expression of cleaved caspase-8 and PARP was markedly reduced upon pretreat-

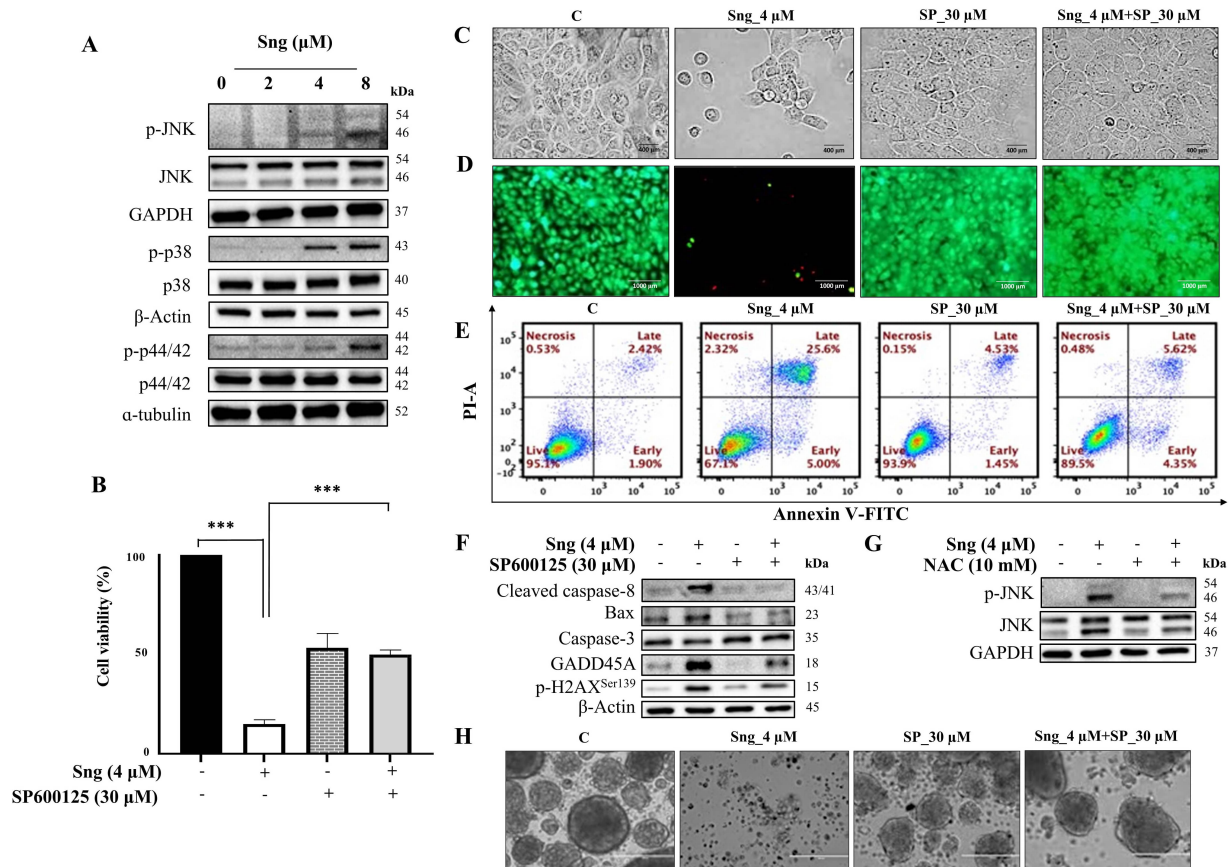


**Fig. 6. Activation of the JNK signaling pathway by Sanguinarine in A388 monolayer cells and spheroids.** (A) Western blot analysis of JNK, p38, and ERK phosphorylation in A388 cells treated with indicated concentrations of Sng for 6 h. (B) Viability assessment of A388 cells treated with or without SP600125 (30  $\mu$ M) by CCK-8 assay. Data presented as the mean  $\pm$  SD from three independent experiments.  $***p < 0.001$  compared with the Sng-treated group; one-way ANOVA followed by Tukey analysis. (C) Microscopic images of A388 cells treated with SP600125 (30  $\mu$ M), either alone or in combination with Sng (4  $\mu$ M) for 6 h (magnification 10 $\times$ ; scale bar: 400  $\mu$ m). (D) Representative fluorescence staining depicting the distribution of live (indicated by green fluorescence) and dead (indicated by red fluorescence) A388 cells following treatment with SP600125 (30  $\mu$ M), either alone or in combination with Sng (4  $\mu$ M) for 24 h (magnification 4 $\times$ ; scale bar: 1000  $\mu$ m). (E) Scatter plots presenting the kinetics of apoptosis in cells co-treated with SP600125 (30  $\mu$ M) and Sng (4  $\mu$ M). A388 cells were pretreated with SP600125 for 2 h before being challenged with Sng and then stained with Annexin V-FITC/PI after 24 h. The percentage of apoptotic (early and late) cells appears as a readout of enhanced apoptosis in Sng-treated cells but is only partially detectable in SP600125 and Sng co-treated cells. (F) Western blot analysis of apoptotic proteins, cell-cycle regulatory protein, and DNA double-strand break (DSB) indicator in A388 cells treated with SP600125 (30  $\mu$ M) for 2 h prior to treatment with Sng (4  $\mu$ M) for 6 h. (G) Western blot analysis of JNK phosphorylation in A388 cells in response to pretreatment with NAC (10 mM) followed by Sng (4  $\mu$ M) for 6 h. (H) Inhibition of dissolution and apoptosis in A388 spontaneously-forming spheroids on pretreatment with SP600125 (magnification 10 $\times$ ; scale bar: 400  $\mu$ m).

ment with NAC compared to cells treated with Sng alone (Fig. 4K,M). In 3D spheroid cultures, dissolution, the loss of well-circumscribed edges of normally compact cell aggregates, corresponds to the induction of apoptosis [43]. Interestingly, the dissolution of metastatic A388 cell-derived multicellular spheroids was also inhibited by NAC treatment alone or in combination with Sng (Fig. 4L).

To further investigate the role of ROS in caspase-mediated cell death, we analyzed changes in intracellular and mitochondrial ROS levels in A388 cells pretreated with z-VAD-FMK. Both intracellular and mitochondrial ROS

production were significantly reduced upon pretreatment with z-VAD-FMK. In contrast, they remained more or less unchanged in cells treated with either z-VAD-FMK or Sng alone (Supplementary Fig. 3a,b). These findings emphasize the functional role of the caspase-dependent pathway in Sng-induced apoptosis, which is secondary to the modulation of ROS.

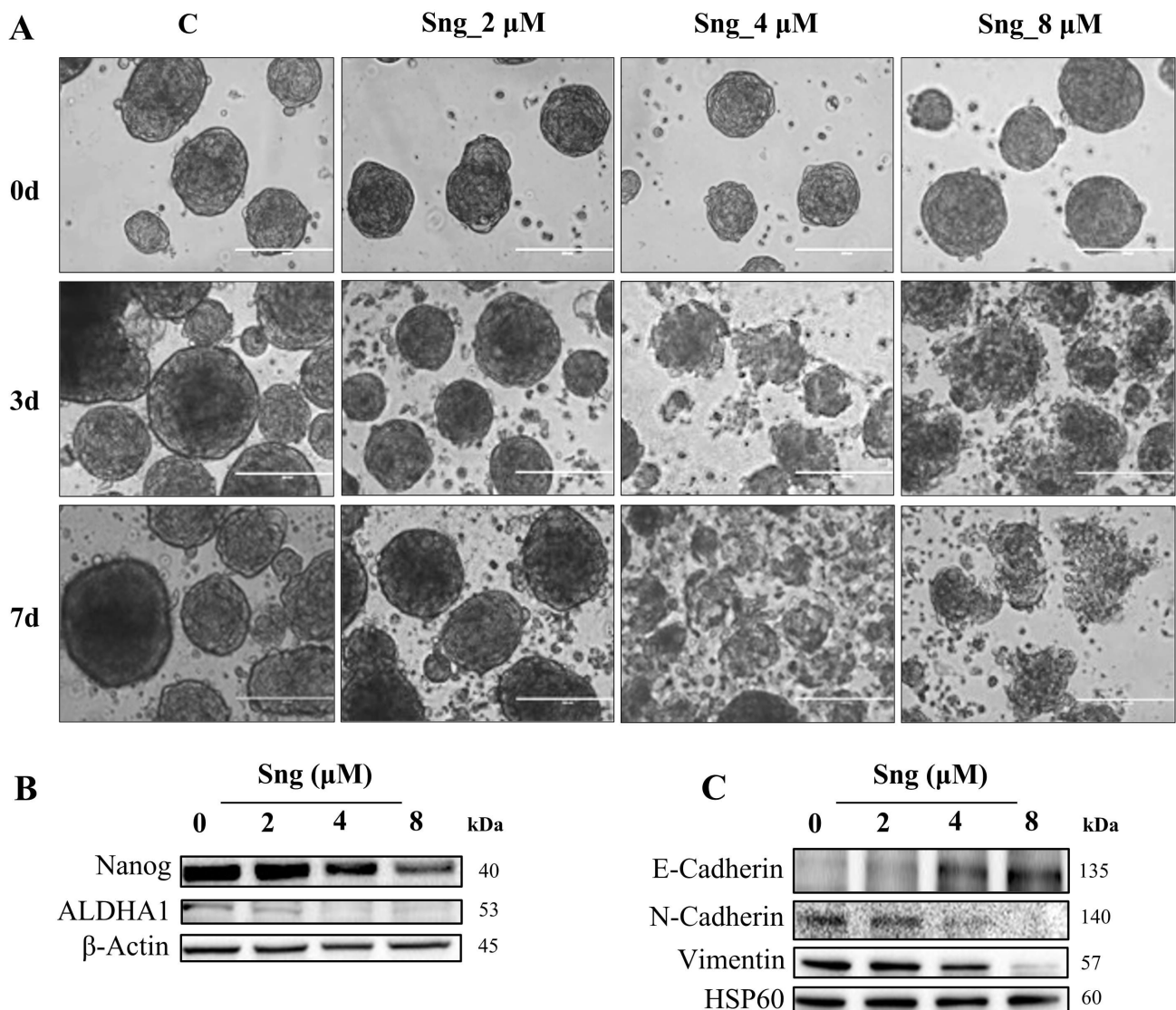


**Fig. 7. Ablation of stemness potential by Sanguinarine in metastatic cSCC cells.** (A) Representative optical images of A388 cell-derived spheroids that were systematically investigated for the effect of Sng on spheroidal dissolution and apoptosis at 0, 3, and 7 cultivation days (magnification 10×; scale bar: 400 μm). (B) Expression profile of the stemness gene and CSC cell surface marker in A388 spheroids. (C) Expression profile of EMT-associated markers in A388 spheroids. CSC, cancer stem cell; EMT, Epithelial-Mesenchymal Transition.

### 3.4 Sanguinarine Disrupts the Mitochondrial Membrane Potential ( $\Delta\Psi_m$ ) and Evokes Mitochondria-Mediated Apoptosis in cSCC Cells

Sng has been previously shown to elevate ROS levels in neoplastic cells, thereby disrupting redox homeostasis and inducing oxidative stress [21,26]. Because oxidative stress can occur at either a high  $\Delta\Psi_m$  or low  $\Delta\Psi_m$  [44], we assessed the capacity of Sng to alter  $\Delta\Psi_m$  in A388 and A431 cells. As shown in Fig. 5A,B, Sng induces a progressive loss of  $\Delta\Psi_m$  in cSCC cells, as manifested by the right-shift peak reflecting the increased number of cells with dissipated  $\Delta\Psi_m$ . Additionally, co-treatment of A388 cells with NAC moderately restored  $\Delta\Psi_m$  compared to the loss induced by Sng alone (Supplementary Fig. 4c). In

addition, we ascertained whether z-VAD-FMK maintains  $\Delta\Psi_m$ . Flow cytometric analysis showed that z-VAD-FMK pretreatment moderated the dissipation of  $\Delta\Psi_m$  compared to the loss induced by Sng alone (Supplementary Fig. 3d).

The fact that alterations in mitochondrial energization, particularly the loss of  $\Delta\Psi_m$ , trigger the translocation of the cytosolic pro-apoptotic Bcl-2 family member Bax to the mitochondria [45] prompted us to determine the levels of Bax in cSCC cells treated with Sng. We demonstrated that the exposure of A431 cells to increasing concentrations of Sng for 6 h increased the levels of Bax protein (Fig. 5D). However, in A388 cells, the expression of Bax gradually increased, with maximal expression at 4 μM Sng (Fig. 5C). Sng-treated cSCC cells were also examined for the expres-

sion of other intrinsic apoptotic death regulators involved in maintaining mitochondrial membrane integrity. Given that the pro-apoptotic effector Bid cooperates with Bax in mitochondrial dysfunction [46], we assessed the expression of Bid. In the case of A431 cells treated with indicated concentrations of Sng for 6 h, the expression of inactive full-length Bid gradually decreased with concentration, whereas maximal expression of the active large fragment of Bid (tBid) was observed in cells exposed to 4  $\mu$ M of Sng (Fig. 5D). Similar to Bax expression in A388 cells, a gradual increase in the expression of inactive full-length Bid was observed, with maximal expression achieved post-treatment with 4  $\mu$ M Sng (Fig. 5C) [47]. We also determined the expression of caspase-9 in response to Sng-induced mitochondrial membrane defects. As shown in Fig. 5C,D, an increase in caspase-9 activity in A388 (relatively higher at 4  $\mu$ M Sng) and A431 (somewhat higher at 8  $\mu$ M Sng) cells was observed. Taken together, Sng generates a potent intrinsic apoptotic stimulus and induces  $\Delta\Psi_m$  dysfunction, indicative of its mitochondrial-targeting potential.

### 3.5 Sanguinarine Induces Apoptosis in cSCC Cells via Modulating the Mitogen-Activated Protein Kinase (MAPK) Signaling Pathway

Substantial evidence has highlighted the pivotal role of MAPKs in regulating stimulus-specific cellular responses, including cell growth, migration, proliferation, differentiation, and apoptosis [48]. To elucidate the possible link between apoptosis and the MAPK pathway in cSCC cells, we investigated the influence of Sng on the MAPK signaling pathways in A388 cells. Indeed, Sng promoted the phosphorylation and activation of JNK, p38, and ERK (p44/42 MAPK), with maximal phosphorylation (specifically that of JNK and ERK) observed at 8  $\mu$ M Sng (Fig. 6A), thus corroborating the involvement of MAPKs in Sng-induced apoptosis in A388 cells. The expression of JNK, p38, and ERK remained unchanged. Following this observation, we investigated the impact of SB203580 (a p38 inhibitor), U0126 (an ERK1/2 inhibitor), and SP600125 (a JNK inhibitor) on MAPK signaling-mediated caspase-dependent apoptosis in A388 cells. According to the trypan blue assay, the Sng-induced decrease in viable A388 cells was not restored upon the pretreatment with SB203580 and U0126 (**Supplementary Fig. 5a,b**). SB203580/Sng co-treatment inhibited the expression of cleaved caspase-8 and PARP, whereas U0126/Sng co-treatment failed to inhibit the Sng-induced activity of these proteins in A388 cells. Moreover, inhibition of p38 and ERK did not attenuate the Sng-induced H2AX phosphorylation at Ser139, indicating no reversibility of DNA damage prompted by Sng in A388 cells (**Supplementary Fig. 5c,d**).

Earlier studies have delineated the capacity of Sng to induce ROS production and effectively activate the JNK signaling pathway [49]. Therefore, we determined the functional role of JNK signaling in Sng-induced apopto-

sis in cSCC cells using the pharmacological JNK inhibitor SP600125. As shown in Fig. 6B, restoration of cell viability was observed when Sng-treated A388 cells were pre-exposed to SP600125 for 2 h. Viability assessment following inhibition of JNK activity in A431 cells also yielded similar results (data not shown). In A388 cells, pretreatment preserved the morphological characteristics (Fig. 6C) and markedly decreased the number of dead cells compared to the Sng-treated group (Fig. 6D). As derived from flow cytometry analysis (Fig. 6E), SP600125 pretreatment significantly attenuated the accumulation of apoptotic cells relative to cells treated with Sng alone. Furthermore, blocking JNK with SP600125 attenuated the Sng-induced expression of caspase-3, cleaved caspase-8, Bax, GADD45A, and p-H2AX<sup>Ser139</sup> (Fig. 6F).

To elucidate whether ROS are involved in Sng-mediated JNK activation, A388 cells were treated with Sng with or without NAC. Co-treatment of A388 cells with Sng and NAC for 6 h blocked JNK activation relative to those treated with Sng alone (Fig. 6G). These results confirmed the participation of ROS-dependent JNK signaling in the pro-apoptotic effects induced by Sng cSCC cells.

Compared to rescuing parental monolayer cells from the apoptotic effect of Sng, SP600125 also prevented the Sng-induced dissolution of intact spheroids. Both SP600125 and SP600125-Sng co-treated spheroids maintained well-circumscribed edges comparable to those of the control (Fig. 6H), indicating spheroid viability.

### 3.6 Sanguinarine Reduces Stemness in cSCC Cells through Modulation of Cancer Stem Cell (CSC) and Epithelial-Mesenchymal Transition (EMT) Inducer Genes

*In vitro*, 3D tumor spheroid models have emerged as viable tools for drug screening. To analyze the cell response to Sng in 3D culture, we assessed the dissolution of metastatic A388 cell-derived spheroids. The so-called tumor-derived spheroids were generated in a 3D scaffold-free culture system using 2D A388 adherent cells that were grown as floating spheres in an ultra-low attachment 6-well plate and sensitized to increasing concentrations of Sng for 7 days. A388 cells formed dense globe-like aggregates with prominent core formation (Fig. 7A). Following a 7-day treatment period, the dissolution of the spheroids in each well was assessed. At a concentration of 2  $\mu$ M, Sng showed no apoptotic response, as the spheroids retained their well-circumscribed edges identical to the control. This contrasts the higher concentrations of Sng (4 and 8  $\mu$ M), which showed a mixed apoptotic response, characterized by the co-existence of spheroids with significantly distorted edges and single-cell populations (Fig. 7A).

To investigate the effect of Sng on cancer stem cells (CSCs) enriched in the formed spheroids, we assessed the expression of the key stemness gene Nanog and the cell surface marker aldehyde dehydrogenase A1 (ALDH1). Sng-treated A388 spheroids displayed downregulation of both

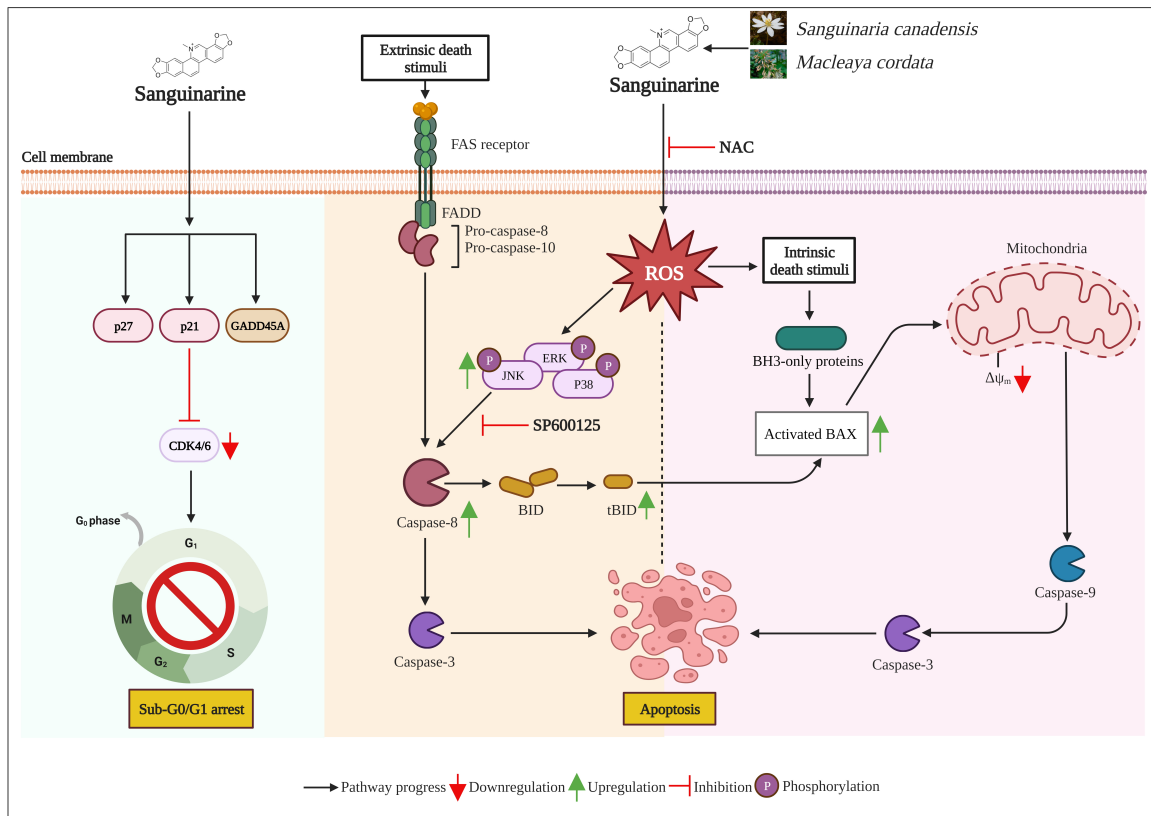


**Fig. 8. Schematic diagram depicting the proposed molecular mechanisms that underscore the anti-cancer activity of Sanguinarine in cSCC cells.** Sng induces sub-G0/G1 arrest and triggers apoptosis by activating the JNK pathway that is dependent on the ROS-mediated signaling in human cSCC cells. CDK, Cyclin-dependent kinase; FADD, Fas Associated Via Death Domain; GADD45A, growth arrest and DNA damage-inducible gene 45 alpha; tBID, truncated bid. Created with [BioRender.com](https://www.biorender.com).

Nanog and ALDH1 expression (Fig. 7B). Epithelial-mesenchymal transition (EMT) is a highly plastic, dynamic transitional process characterized by the loss of apical polarity and gain of mesenchymal properties, cell motility, and stemness in epithelial cells in a variety of cancerous tissues [50]. Considering that EMT confers stem cell-like traits to neoplastic cells, we evaluated the ability of Sng to abrogate the EMT phenotype in A388 spheroids. Western blot analysis demonstrated an increase in the expression levels of the epithelial marker E-cadherin, with concurrent downregulation in the levels of the mesenchymal markers N-cadherin and vimentin upon treatment with Sng (Fig. 7C).

#### 4. Discussion

Growing awareness of the complex dynamics of cSCC in recent decades has widened the understanding of its molecular pathogenesis and, thus, the therapeutic arsenal

against this commonly occurring cutaneous malignancy. However, in comparison to the common primary cSCCs that present indolent clinical behavior and favorable prognosis, the burden of metastatic cSCCs portending poorer prognosis and higher mortality rates (>70%) has emphasized the need for novel therapeutic strategies in this group [51]. Validation of the high mutational burden and immunogenicity of cSCC tumors has resulted in the approval of immune checkpoint inhibitors for this entity [52]. In addition, phytochemicals have evolved as a complementary therapeutic strategy to conventional chemotherapy because of their diverse pharmacological properties, multi-targeting abilities, and anti-cancer potential. The bioactive benzophenanthridine alkaloid Sng exhibits a wide spectrum of therapeutic applications, ranging from antimicrobial to potential anti-cancer activity [53]. In this study, the potential cytotoxic effects of Sng were comprehensively investigated *in vitro* using primary and metastatic cSCC cells. Our

findings, for the first time, demonstrate that Sng mediates anti-cancer actions in cSCC cells through cell cycle arrest and apoptosis via ROS-dependent JNK signaling pathway (Fig. 8).

Drug toxicity can be defined as the combination of two processes: induction of cell death (cytotoxic effect) and inhibition of proliferation and metabolism (cytostatic effect). Consistent with the published literature [54], our study suggests that Sng exerts both cytostatic and cytotoxic effects on cSCC cells. According to the cytotoxicity assays, Sng decreased the number of viable cells and dramatically reduced the clonogenic abilities of both primary and metastatic cSCC cells. Previous experimental observations have demonstrated the preferential cytotoxicity of Sng to A431 cells via apoptosis compared to normal human epidermal keratinocytes [55], thus unraveling the differential growth-inhibitory response of Sng in cancer cells *versus* normal cells. Cellular homeostasis relies on the precise regulation of cellular signaling systems that control the spatial and temporal balance of cell proliferation, growth arrest, and apoptosis [56]. The hub of these signaling systems is the cell cycle, the progression of which is regulated by sequential activation and inactivation of different cyclin/cyclin-dependent kinase (CDK) regulatory complexes [57]. Our study revealed that Sng induces significant sub-G0/G1 cell-cycle arrest in cSCC cells, suggesting that Sng acts via a cell cycle-specific mechanism. Critical to cell cycle exit is the activity of CDK inhibitors, including p21<sup>WAF1</sup> and p27<sup>KIP1</sup>, which inhibit CDK4/6 involved in the G1/S transition [58]. Investigation into cell cycle arrest in the sub-G1 phase showed that Sng relies on the upregulated expression of p21 and p27 to inhibit the activity of CDK6 and block the G1/S cell-cycle transition in primary cSCC cells. The sub-G0/G1 phase arrest induced by Sng was also accompanied by upregulated GADD45A expression in metastatic cSCC cells, suggesting the cytostatic stress generated by Sng. GADD45A is a member of the GADD45 family of genes, which acts as a stress sensor and integrates various stress stimuli into cell cycle arrest via physical interactions with cell cycle regulatory proteins, including p21 [57]. Our findings indicate that cell cycle arrest in metastatic cSCC cells is initiated by the joint upregulation of GADD45A and p21 after Sng treatment. Numerous studies have shown that both GADD45A and p21 can exert their control on cell-cycle machinery in a tumor protein 53 (TP53)-dependent and -independent manner [58]; therefore, the functional significance of TP53 in Sng-induced cell-cycle arrest in metastatic cSCC cells needs to be investigated.

In addition to growth arrest, negative growth rate control, such as apoptosis, is critical in regulating aberrant development in cancer. Apoptosis is a universal, highly complex RCD mode that occurs via two pathways: (a) the extrinsic/death receptor pathway, initiated by perturbations of the extracellular microenvironment that are detected by

activation of cell surface death receptors, propagated by apical caspase (-8), and precipitated by executioner caspases, mainly caspase-3; and (b) the intrinsic/mitochondrial pathway, initiated by perturbations of the intracellular or extracellular microenvironment, demarcated by mitochondrial dysfunction, propagated by apical caspase (-9), and precipitated by caspase-3 [37]. Both pathways converge on the activation of downstream caspases, which are normally expressed as inactive zymogens (procaspases) until stimulation. In the present study, we showed that initiator caspases-8 and -9 and effector caspase-3 are concomitantly activated upon treatment with Sng, suggesting the involvement of both the extrinsic and intrinsic pathways in Sng-induced apoptosis. Caspase inhibition by z-VAD-FMK substantially inhibited Sng-mediated inhibition of cell viability, clonogenic potential, and apoptosis, thus implicating caspase cascades in Sng-mediated apoptosis of cSCC cells. The morphological documentation also revealed the cellular changes typical of apoptosis, which allied with the analysis from flow cytometric Annexin V/PI assay and western blot, suggesting a majorly apoptotic mode of death. Progressive DNA damage, reflected by upregulated p-H2AX<sup>Ser139</sup> levels following the initiation of DNA fragmentation and decreased PARP activity, further proved that the antiproliferative effect of Sng is related to apoptosis induction and DNA damage.

The complex relationship between ROS and cancer depends on the precise fine-tuning of ROS production and scavenging. During carcinogenesis, ROS exhibits a paradoxical role: ectopic ROS accumulation promotes the proliferation and survival of cancer cells via the activation of redox-sensitive signaling pathways, whereas excessive ROS levels promote cell death [59]. Given that reprogramming of redox metabolism can counteract tumorigenesis, our study demonstrated the potential of Sng to serve as a ROS-stimulating agent, overwhelming redox adaptation and inducing oxidative stress in cSCC cells. The loss of  $\Delta\Psi_m$  signifies bioenergetic/oxidative stress and mitochondrial dysfunction, which can contribute to the release of apoptotic factors and induce the intrinsic apoptotic signaling cascade. Our data revealed that  $\Delta\Psi_m$  dissipation was linked to Sng-induced apoptosis in cSCC cells, together with the activation of caspase-9, caspase-3, Bax, and Bid. However, z-VAD-FMK only partially reversed the loss of  $\Delta\Psi_m$ , indicating that its initial loss was independent of caspases. Similarly,  $\Delta\Psi_m$  dissipation was partially prevented by the application of NAC, suggesting that the Sng-induced redox imbalance occurs before the loss of  $\Delta\Psi_m$  and caspase-3 activation. Sng also depleted the levels of GSH, a tripeptide of the intracellular antioxidative system, in cSCC cells, thereby disturbing oxidant-antioxidant dynamics and making cells more susceptible to oxidative stress. The mechanism underlying the Sng-mediated depletion of GSH is unclear. Still, it can be attributed to its ability to bind to intracellular GSH, as demonstrated in the

case of other phytochemicals [60]. Blocking ROS generation with NAC restored GSH levels and abolished Sng-induced apoptosis in both monolayer and spheroid cultures. The protective effect of NAC, owing to ROS scavenging and GSH depletion, corroborated that an oxidative stress-related mechanism mediated the intrinsic apoptotic signaling cascade induced by Sng in cSCC cells.

Ser/Thr protein kinases, such as JNKs, are components of the “three-tiered” MAPK signaling that mediate an array of cellular responses, including cell survival and apoptosis, in response to a variety of abiotic and biotic stress insults, such as oxidative stress and DNA damage [61]. In this study, we demonstrated that JNK is an important mediator of cytotoxic damage induced by Sng in both monolayer and spheroid cultures of metastatic cSCC cells. The cytotoxic effect of Sng significantly increased the phosphorylation of JNK in metastatic cSCC cells. In contrast, the pharmacological inhibition of JNK protected the cells from Sng-induced cytotoxicity *in vitro* and attenuated the expression of caspase-3 and cleaved caspase-8. Inhibition of JNK activation also reversed the Sng-induced expression of p-H2AX and GADD45A, thus linking previously thought unrelated phenomena, that is, the DNA damage-induced expression of GADD45-like genes and the DNA damage-induced activation of the JNK pathway. In addition to cell cycle arrest, GADD45 proteins have been implicated in DNA damage and environmental stress-related responses via the activation of the MEKK4/p38/JNK signaling pathway [62]. Moreover, JNK inhibition downregulated the expression of Bax, thus connecting the stress-activated signaling pathway to the cell death machinery involved in mitochondrial apoptosis. Furthermore, the ROS scavenger NAC preserved Sng-induced JNK phosphorylation, suggesting the involvement of ROS/JNK pathway in Sng-induced apoptosis of metastatic cSCC cells.

Effect of Sng on spheroids revealed the possible potency of the drug in addition to traditional 2D monolayer cultures. Sng treatment elicited a mixed apoptotic response in 3D spheroids, as indicated by the co-existence of partially dissolute spheroids and single-cell populations. This response can be attributed to Sng targeting only proliferative cells predominantly residing in the peripheral zone of the spheroids. Future studies assessing the penetration of Sng into spheroids are required to determine whether it is one of the causal factors underlying the limited response of Sng. Nevertheless, Sng displayed considerable potency against cSCC cell-derived spheroids. Tumor-derived spheroids have been widely used to enrich putative CSCs and evaluate stem cell-like properties *in vitro*. Amidst the current focus on developing therapeutic strategies to target and eliminate CSCs to counteract drug resistance and tumor recurrence, our study revealed that the stemness-targeting ability of Sng was prompted by the downregulation of Nanog and ALDH1. Moreover, considering that EMT and CSCs belong to the triad of major contributing factors of metastasis

and are interlinked [63], we also demonstrated the capacity of Sng to target EMT effector molecules in tumorspheres obtained from metastatic cSCC cells.

## 5. Conclusion

In conclusion, our study explored the anti-cancer potential of Sng against cSCC cells, which is mediated through cell-cycle arrest leading to apoptosis via the ROS/JNK signaling pathway. In view of its chemosensitive abilities *in vitro*, the cytotoxic potential of Sng, at relatively lower dosages, requires further evaluation in animal efficacy models. Moreover, investigations into the pharmacologic synergy and efficacy between Sng and other phytochemicals and/or traditional chemotherapeutic drugs are warranted to identify, test, and develop an efficacious clinically relevant combinatorial drug regimen against cSCC.

## Availability of Data and Materials

This published article and its supplementary information files include all data generated and/or analysed during this study.

## Author Contributions

MS and SU designed and supervised the research and coordinated the project. KP conducted the main experiments. KP, SU and MS wrote the manuscript. AQK, FA, SK, RA, JMM and AAB helped in drafting the manuscript, critically reviewing it, data analyzing. AA, AAB and JB involved in designing, performing analysis of the data as well helped in writing of the manuscript. All authors read and approved the final manuscript. All authors have participated sufficiently in the work and agreed to be accountable for all aspects of the work.

## Ethics Approval and Consent to Participate

Not applicable.

## Acknowledgment

Not applicable.

## Funding

This study was funded by Medical Research Center, Hamad Medical Corporation, under grant no. MRC-01-23-065.

## Conflict of Interest

Given his role as a guest editor, Dr. Shahab Uddin had no involvement in the peer-review of this article and has no access to information regarding its peer review. Full responsibility for the editorial process for this article was delegated to Prof. Amancio Carnero Moya. The other authors have no conflict of interest.

## Supplementary Material

Supplementary material associated with this article can be found, in the online version, at <https://doi.org/10.31083/j.fbl2901040>.

## References

- [1] Smoller BR. Squamous cell carcinoma: from precursor lesions to high-risk variants. *Modern Pathology*. 2006; 19: S88–S92.
- [2] Rubió-Casadevall J, Hernandez-Pujol AM, Ferreira-Santos MC, Morey-Esteve G, Vilardell L, Osca-Gelis G, *et al*. Trends in incidence and survival analysis in non-melanoma skin cancer from 1994 to 2012 in Girona, Spain: A population-based study. *Cancer Epidemiology*. 2016; 45: 6–10.
- [3] Goon PKC, Greenberg DC, Igal L, Levell NJ. Squamous Cell Carcinoma of the Skin has More Than Doubled Over the Last Decade in the UK. *Acta Dermato-Venereologica*. 2016; 96: 820–821.
- [4] Rogers HW, Weinstock MA, Feldman SR, Coldiron BM. Incidence Estimate of Nonmelanoma Skin Cancer (Keratinocyte Carcinomas) in the U.S. Population, 2012. *JAMA Dermatology*. 2015; 151: 1081–1086.
- [5] Robsahm TE, Helsing P, Veierød MB. Cutaneous squamous cell carcinoma in Norway 1963–2011: increasing incidence and stable mortality. *Cancer Medicine*. 2015; 4: 472–480.
- [6] Perera E, Gnaneswaran N, Staines C, Win AK, Sinclair R. Incidence and prevalence of non-melanoma skin cancer in Australia: A systematic review. *The Australasian Journal of Dermatology*. 2015; 56: 258–267.
- [7] Thiem DGE, Scharr K, Pabst AM, Saka B, Kämmerer PW. Facial cutaneous squamous cell carcinoma - microscopic safety margins and their impact on developing local recurrences. *Journal of Cranio-Maxillo-Facial Surgery*. 2020; 48: 49–55.
- [8] Corchado-Cobos R, García-Sancha N, González-Sarmiento R, Pérez-Losada J, Cañueto J. Cutaneous Squamous Cell Carcinoma: From Biology to Therapy. *International Journal of Molecular Sciences*. 2020; 21: 2956.
- [9] Ratushny V, Gober MD, Hick R, Ridky TW, Seykora JT. From keratinocyte to cancer: the pathogenesis and modeling of cutaneous squamous cell carcinoma. *The Journal of Clinical Investigation*. 2012; 122: 464–472.
- [10] Stratigos AJ, Garbe C, Dessinioti C, Lebbe C, Bataille V, Bastholt L, *et al*. European interdisciplinary guideline on invasive squamous cell carcinoma of the skin: Part 1. epidemiology, diagnostics and prevention. *European Journal of Cancer*. 2020; 128: 60–82.
- [11] Inman GJ, Wang J, Nagano A, Alexandrov LB, Purdie KJ, Taylor RG, *et al*. The genomic landscape of cutaneous SCC reveals drivers and a novel azathioprine associated mutational signature. *Nature Communications*. 2018; 9: 3667.
- [12] Schmults CD, Blitzblau R, Aasi SZ, Alam M, Andersen JS, Baumann BC, *et al*. NCCN Guidelines® Insights: Squamous Cell Skin Cancer, Version 1.2022. *Journal of the National Comprehensive Cancer Network*. 2021; 19: 1382–1394.
- [13] Millsop JW, Sivamani RK, Fazel N. Botanical agents for the treatment of nonmelanoma skin cancer. *Dermatology Research and Practice*. 2013; 2013: 837152.
- [14] Lebowhl M, Swanson N, Anderson LL, Melgaard A, Xu Z, Berman B. Ingenol mebutate gel for actinic keratosis. *The New England Journal of Medicine*. 2012; 366: 1010–1019.
- [15] Fidler B, Goldberg T. Ingenol mebutate gel (picato): a novel agent for the treatment of actinic keratoses. *Pharmacy and Therapeutics*. 2014; 39: 40–46.
- [16] Phillips JM, Clark C, Herman-Ferdinandez L, Moore-Medlin T, Rong X, Gill JR, *et al*. Curcumin inhibits skin squamous cell carcinoma tumor growth in vivo. *Otolaryngology–head and Neck Surgery*. 2011; 145: 58–63.
- [17] Achkar IW, Mraiche F, Mohammad RM, Uddin S. Anticancer potential of sanguinarine for various human malignancies. *Future Medicinal Chemistry*. 2017; 9: 933–950.
- [18] Han MH, Kim GY, Yoo YH, Choi YH. Sanguinarine induces apoptosis in human colorectal cancer HCT-116 cells through ROS-mediated Egr-1 activation and mitochondrial dysfunction. *Toxicology Letters*. 2013; 220: 157–166.
- [19] Wang Y, Zhang B, Liu W, Dai Y, Shi Y, Zeng Q, *et al*. Noninvasive bioluminescence imaging of the dynamics of sanguinarine induced apoptosis via activation of reactive oxygen species. *Oncotarget*. 2016; 7: 22355–22367.
- [20] Prabhu KS, Bhat AA, Siveen KS, Kuttikrishnan S, Raza SS, Raheed T, *et al*. Sanguinarine mediated apoptosis in Non-Small Cell Lung Cancer via generation of reactive oxygen species and suppression of JAK/STAT pathway. *Biomedicine & Pharmacotherapy*. 2021; 144: 112358.
- [21] Hussain AR, Al-Jomah NA, Siraj AK, Manogaran P, Al-Hussein K, Abubaker J, *et al*. Sanguinarine-dependent induction of apoptosis in primary effusion lymphoma cells. *Cancer Research*. 2007; 67: 3888–3897.
- [22] Al-Tamimi M, Khan AQ, Anver R, Ahmad F, M Mateo J, Raza SS, *et al*. Pristimerin mediated anticancer effects and sensitization of human skin cancer cells through modulation of MAPK signaling pathways. *Biomedicine & Pharmacotherapy*. 2022; 156: 113950.
- [23] Eun JP, Koh GY. Suppression of angiogenesis by the plant alkaloid, sanguinarine. *Biochemical and Biophysical Research Communications*. 2004; 317: 618–624.
- [24] Reagan-Shaw S, Breur J, Ahmad N. Enhancement of UVB radiation-mediated apoptosis by sanguinarine in HaCaT human immortalized keratinocytes. *Molecular Cancer Therapeutics*. 2006; 5: 418–429.
- [25] Ahsan H, Reagan-Shaw S, Eggert DM, Tan TC, Afaq F, Mukhtar H, *et al*. Protective effect of sanguinarine on ultraviolet B-mediated damages in SKH-1 hairless mouse skin: implications for prevention of skin cancer. *Photochemistry and Photobiology*. 2007; 83: 986–993.
- [26] Khan AQ, Mohamed EAN, Hakeem I, Nazeer A, Kuttikrishnan S, Prabhu KS, *et al*. Sanguinarine Induces Apoptosis in Papillary Thyroid Cancer Cells via Generation of Reactive Oxygen Species. *Molecules*. 2020; 25: 1229.
- [27] Strober W. Trypan Blue Exclusion Test of Cell Viability. *Current Protocols in Immunology*. 2015; 111: A3.B.1–A3.B.3.
- [28] Hussain AR, Uddin S, Ahmed M, Bu R, Ahmed SO, Abubaker J, *et al*. Prognostic significance of XIAP expression in DLBCL and effect of its inhibition on AKT signalling. *The Journal of Pathology*. 2010; 222: 180–190.
- [29] Uddin S, Hussain AR, Ahmed M, Siddiqui K, Al-Dayel F, Bavi P, *et al*. Overexpression of FoxM1 offers a promising therapeutic target in diffuse large B-cell lymphoma. *Haematologica*. 2012; 97: 1092–1100.
- [30] Iskandarani A, Bhat AA, Siveen KS, Prabhu KS, Kuttikrishnan S, Khan MA, *et al*. Bortezomib-mediated downregulation of S-phase kinase protein-2 (SKP2) causes apoptotic cell death in chronic myelogenous leukemia cells. *Journal of Translational Medicine*. 2016; 14: 69.
- [31] Bodle CR, Mackie DI, Hayes MP, Schamp JH, Miller MR, Henry MD, *et al*. Natural Products Discovered in a High-Throughput Screen Identified as Inhibitors of RGS17 and as Cytostatic and Cytotoxic Agents for Lung and Prostate Cancer Cell Lines. *Journal of Natural Products*. 2017; 80: 1992–2000.
- [32] Wei G, Xu Y, Peng T, Yan J, Wang Z, Sun Z. Sanguinarine exhibits antitumor activity via up-regulation of Fas-associated factor 1 in non-small cell lung cancer. *Journal of Biochemical and Molecular Toxicology*. 2017; 31: 10.1002/jbt.21914.



- [33] Gaziano R, Moroni G, Buè C, Miele MT, Sinibaldi-Vallebona P, Pica F. Antitumor effects of the benzophenanthridine alkaloid sanguinarine: Evidence and perspectives. *World Journal of Gastrointestinal Oncology*. 2016; 8: 30–39.
- [34] Kalogris C, Garulli C, Pietrella L, Gambini V, Pucciarelli S, Lucci C, *et al*. Sanguinarine suppresses basal-like breast cancer growth through dihydrofolate reductase inhibition. *Biochemical Pharmacology*. 2014; 90: 226–234.
- [35] De Stefano I, Raspaglio G, Zannoni GF, Travaglia D, Prisco MG, Mosca M, *et al*. Antiproliferative and antiangiogenic effects of the benzophenanthridine alkaloid sanguinarine in melanoma. *Biochemical Pharmacology*. 2009; 78: 1374–1381.
- [36] Stefanowicz-Hajduk J, Ochocka JR. Real-time cell analysis system in cytotoxicity applications: Usefulness and comparison with tetrazolium salt assays. *Toxicology Reports*. 2020; 7: 335–344.
- [37] Galluzzi L, Vitale I, Aaronson SA, Abrams JM, Adam D, Agostinis P, *et al*. Molecular mechanisms of cell death: recommendations of the Nomenclature Committee on Cell Death 2018. *Cell Death & Differentiation*. 2018; 25: 486–541.
- [38] Akhtar S, Achkar IW, Siveen KS, Kuttikrishnan S, Prabhu KS, Khan AQ, *et al*. Sanguinarine Induces Apoptosis Pathway in Multiple Myeloma Cell Lines via Inhibition of the JAK2/STAT3 Signaling. *Frontiers in Oncology*. 2019; 9: 285.
- [39] Bao Q, Shi Y. Apoptosome: a platform for the activation of initiator caspases. *Cell Death and Differentiation*. 2007; 14: 56–65.
- [40] Mah LJ, El-Osta A, Karagiannis TC. gammaH2AX: a sensitive molecular marker of DNA damage and repair. *Leukemia*. 2010; 24: 679–686.
- [41] McStay GP, Green DR. Identification of active caspases using affinity-based probes. *Cold Spring Harbor Protocols*. 2014; 2014: 856–860.
- [42] Nakamura H, Takada K. Reactive oxygen species in cancer: Current findings and future directions. *Cancer Science*. 2021; 112: 3945–3952.
- [43] Alpaugh ML, Barsky SH. Reversible model of spheroid formation allows for high efficiency of gene delivery *ex vivo* and accurate gene assessment *in vivo*. *Human Gene Therapy*. 2002; 13: 1245–1258.
- [44] Aon MA, Cortassa S, O'Rourke B. Redox-optimized ROS balance: a unifying hypothesis. *Biochimica et Biophysica Acta*. 2010; 1797: 865–877.
- [45] Smaili SS, Hsu YT, Sanders KM, Russell JT, Youle RJ. Bax translocation to mitochondria subsequent to a rapid loss of mitochondrial membrane potential. *Cell Death and Differentiation*. 2001; 8: 909–920.
- [46] Bhattacharjee M, Acharya S, Ghosh A, Sarkar P, Chatterjee S, Kumar P, *et al*. Bax and Bid act in synergy to bring about T11TS-mediated glioma apoptosis via the release of mitochondrial cytochrome c and subsequent caspase activation. *International Immunology*. 2008; 20: 1489–1505.
- [47] Brentnall M, Rodriguez-Menocal L, De Guevara RL, Cepero E, Boise LH. Caspase-9, caspase-3 and caspase-7 have distinct roles during intrinsic apoptosis. *BMC Cell Biology*. 2013; 14: 32.
- [48] Cargnello M, Roux PP. Activation and function of the MAPKs and their substrates, the MAPK-activated protein kinases. *Microbiology and Molecular Biology Reviews*. 2011; 75: 50–83.
- [49] Han MH, Park C, Jin CY, Kim GY, Chang YC, Moon SK, *et al*. Apoptosis induction of human bladder cancer cells by sanguinarine through reactive oxygen species-mediated up-regulation of early growth response gene-1. *PLoS ONE*. 2013; 8: e63425.
- [50] Huang Y, Hong W, Wei X. The molecular mechanisms and therapeutic strategies of EMT in tumor progression and metastasis. *Journal of Hematology & Oncology*. 2022; 15: 129.
- [51] Caudill J, Thomas JE, Burkhart CG. The risk of metastases from squamous cell carcinoma of the skin. *International Journal of Dermatology*. 2023; 62: 483–486.
- [52] Stratigos AJ, Garbe C, Dessinioti C, Lebbe C, Bataille V, Bastholt L, *et al*. European interdisciplinary guideline on invasive squamous cell carcinoma of the skin: Part 2. Treatment. *European Journal of Cancer*. 2020; 128: 83–102.
- [53] Galadari S, Rahman A, Pallichankandy S, Thayyullathil F. Molecular targets and anticancer potential of sanguinarine-a benzophenanthridine alkaloid. *Phytomedicine*. 2017; 34: 143–153.
- [54] Singh N, Sharma B. Toxicological Effects of Berberine and Sanguinarine. *Frontiers in Molecular Biosciences*. 2018; 5: 21.
- [55] Ahmad N, Gupta S, Husain MM, Heiskanen KM, Mukhtar H. Differential antiproliferative and apoptotic response of sanguinarine for cancer cells versus normal cells. *Clinical Cancer Research*. 2000; 6: 1524–1528.
- [56] Weinberg WC, Denning MF. P21Waf1 control of epithelial cell cycle and cell fate. *Critical Reviews in Oral Biology and Medicine*. 2002; 13: 453–464.
- [57] Barnum KJ, O'Connell MJ. Cell cycle regulation by checkpoints. *Methods in Molecular Biology*. 2014; 1170: 29–40.
- [58] Pack LR, Daigh LH, Meyer T. Putting the brakes on the cell cycle: mechanisms of cellular growth arrest. *Current Opinion in Cell Biology*. 2019; 60: 106–113.
- [59] Domenicotti C, Marengo B. Paradox Role of Oxidative Stress in Cancer: State of the Art. *Antioxidants*. 2022; 11: 1027.
- [60] Yu ZY, Liang YG, Xiao H, Shan YJ, Dong B, Huang R, *et al*. Melissoidesin G, a diterpenoid purified from *Isodon melissoides*, induces leukemic-cell apoptosis through induction of redox imbalance and exhibits synergy with other anticancer agents. *International Journal of Cancer*. 2007; 121: 2084–2094.
- [61] Zeke A, Misheva M, Reményi A, Bogoyevitch MA. JNK Signaling: Regulation and Functions Based on Complex Protein-Protein Partnerships. *Microbiology and Molecular Biology Reviews*. 2016; 80: 793–835.
- [62] Takekawa M, Saito H. A family of stress-inducible GADD45-like proteins mediate activation of the stress-responsive MTK1/MEKK4 MAPKKK. *Cell*. 1998; 95: 521–530.
- [63] Babaei G, Aziz SGG, Jaghi NZZ. EMT, cancer stem cells and autophagy; The three main axes of metastasis. *Biomedicine & Pharmacotherapy*. 2021; 133: 110909.